Automatic Classification of Winding Asymmetries in Wound Rotor Induction Motors based on Bicoherence and Fuzzy C-Means Algorithms of Stray Flux Signals

Miguel Enrique Iglesias-Martínez, Jose A. Antonino-Daviu, *Senior Member, IEEE*, Pedro Fernández de Córdoba, J. Alberto Conejero and L. Dunai, *Member, IEEE*

***Abstract*—Wound rotor induction motors are used in a certain number of industrial applications due to their interesting advantages, such as the possibility of inserting external rheostats in series with the rotor winding to enhance the torque characteristics under starting and to decrease the high inrush currents. However, the more complex structure of the rotor winding, compared to cage induction motors, is a source for potential maintenance problems. In this regard, several anomalies can lead to the occurrence of asymmetries in the rotor winding that may yield terrible repercussions for the machine's integrity. Therefore, monitoring the levels of asymmetry in the rotor winding is of paramount importance to ensure the correct operation of the motor. This work proposes the use of Bicoherence of the stray flux signal, as an indicator to obtain an automatic classification of the rotor winding condition. For this, the Fuzzy C-Means machine learning algorithm is used, which starts with the Bicoherence calculation and generates the different clusters for grouping and classification, according to the level of winding asymmetry. In addition, an analysis regarding the influence of the flux sensor position on the automatic classification and the failure detection is carried out. The results are highly satisfactory and prove the potential of the method for its future incorporation in autonomous condition monitoring systems that can be satisfactorily applied to determine the health of these machines.**

***Index Terms*—Fault Diagnosis, Asymmetries, Bicoherence, Fuzzy C-Means.**

I. Introduction

Wound rotor induction motors (WRIM) are typically employed in large power industrial applications (above 1,000 hp) due to their interesting advantages: on the one hand, their rotor winding, based on a set of short-circuited coils, can be accessed externally, a fact that enables the measurement of rotor currents, which can be useful for diagnostic purposes. On the other hand, this winding structure enables the insertion of external resistors which modify the speed-torque characteristic of the machine, yielding higher starting torques while maintaining a low value of inrush current [1]. These advantages make them an ideal option for applications involving ball and sag mills, cranes, pumps, fans and blowers, chippers, hoists and conveyors, among others [1].

In spite of these advantages, they are much less widespread compared to cage induction motors since, among other facts, their more complex rotor winding structure causes notable maintenance problems. As reported in [2], damages in the rotor winding may appear in the end region due to centrifugal forces on the crossovers and connections of the winding causing shorts between turns. On the other hand, it is also common to find asymmetries in the three-phase rotor winding caused by a diversity of reasons: uneven contacts between slip rings and brushes caused by incorrect tightening or uneven wearing, high resistance connections between phase coils, unbalances in the external resistors…[2]. A field example of this common failure was reported in [3], where a rotor asymmetry in a 12P, 3.3kV, 1,500 kW WRIM driving a ball mill was detected. After a

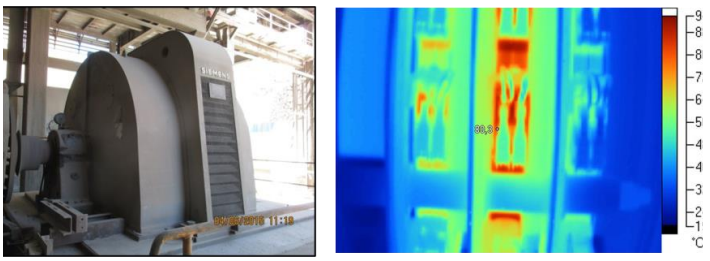

Fig. 1. Rotor asymmetry reported in a field WRIM [3]: WRIM (left) and infrared picture of the slip rings/brushes system (right).

This work was supported in part by Generalitat Valenciana, Conselleria de Innovacion, Universidades, Ciencia y Sociedad Digital, (project AICO/019/224) and in part by MEC under Project MTM 2016-7963-P.

M. E. Iglesias-Martínez is with the Departamento de Telecomunicaciones, Universidad de Pinar del Río Hermanos Saíz Montes de Oca, Pinar del Río 20100, Cuba (e-mail: migueliglesias2010@gmail.com), and with InterTech Interdisciplinary Modeling Group from the Instituto Universitario de Matemática Pura y Aplicada, Universitat Politècnica de València, Valencia E-46022, Spain (email: miigmar@doctor.upv.es)

J. A. Antonino-Daviu is with the Instituto Tecnológico de la Energía, Universitat Politècnica de València, Valencia E-46022, Spain (e-mail: joanda@die.upv.es).

P. Fernández de Córdoba and J. A. Conejero are with the Instituto Universitario de Matemática Pura y Aplicada, Universitat Politècnica de València, Valencia E-46022, Spain (e-mail: pfernandez@mat.upv.es; aconejero@upv.es).

L. Dunai is with the Centro de Investigación en Tecnologías Gráficas, Universitat Politècnica de València, Valencia, SPAIN (e-mail: ladu@upv.es).

.

thorough investigation, the asymmetry was attributed to a defective contact between the slip ring and brushes of one rotor phase, which caused abnormal heat dissipations (a temperature difference of 30ºC versus the rest of phases) that could have led to a catastrophic failure if it had remained undetected. Fig. 1 shows some pictures of this field case [3]. In spite that the likelihood of rotor asymmetries is higher in WRIM compared to cage IM, there are fewer works addressed to these machines. Despite this, several interesting approaches to detect rotor winding asymmetries in WRIM have been proposed in the recent literature [3]-[7]; this proves the interest of this type of machines and the relevance of developing reliable methods to determine the condition of the rotor winding.

This paper is focused on the use of the study of the stray flux under starting with the aim of detecting rotor asymmetries in WRIM. The study of the stray flux has recently drawn a renewed attention from many researchers and companies of the electric motors condition monitoring area due to the interesting advantages of the technique compared to other methods: simplicity, low cost, non-invasive nature and useful informational source for the discrimination between some faults (e.g. eccentricities/unbalances [4]) and for avoiding false indications (e.g. cooling axial ducts). In this regard, the analysis of stray flux signals has proven to provide much richer information than the analysis of other quantities, such as currents, which is the quantity that has been considered in most of past works dealing with WRIM [5]-[7]. On the other hand, despite the technique has still some issues to be solved such as the influence of sensor position on the results, it has also a huge potential derived, indeed, from this fact: combining the information from different sensor locations that capture different flux portions (axial and /or radial), it is possible to enhance the reliability of the diagnosis that can rely on multiple harmonics of different nature (axial and radial), as it has been proven in recent works [8]-[9].

Over recent years, the research has moved a step forward and it has been proven that the analysis of the stray flux under starting with suitable time-frequency transforms yields characteristic patterns caused by the transient evolutions of the fault components. These are very reliable evidences of the presence of those faults. This recent diagnosis approach has been applied with success to detect rotor damages and mechanical faults in cage induction motors [4], [8] and even some works have proven the suitability of this method to detect rotor asymmetries in WRIM [9]. In spite of these advances, the application of the stray-flux-based technique still relies on the user expertness to interpret the time-frequency maps and to identify the fault components' evolutions; for instance, the method proposed in [9], though powerful, mainly relies on the qualitative interpretation of the time-frequency maps resulting from the application of the proposed tools. It does not include automatic classification algorithms for rotor winding asymmetry diagnosis, which would make the fault detection independent from the user expertise and which would facilitate the implementation of the methodology in portable condition monitoring devices or autonomous diagnosis systems.

The present work is aimed to provide a solution to these pending issues by proposing the computation of the Bicoherence of the stray flux signals under motor starting for the detection of rotor winding asymmetries. In relation to the use of Bicoherence in faults diagnosis, different works have been carried out [10]-[12]; most of these rely on the use of the vibration signals and deal with other types of motors [13]. Other works, such as [14]-[16], use wavelet coherence to identify nonlinearities in dynamic systems. In [17], wavelet coherence is used for the identification of faults in electromechanical systems. Some of these works make use of current signals, in addition to vibration signals but none of them has proposed the utilization of stray flux signals. The approach presented in this paper for the automatic identification of asymmetries relies on the combination of high-order spectral analysis with an unsupervised learning technique as the fuzzy C-Mean algorithm which means an important improvement of the results presented in [18]. The results prove the potential of the method for the automatic fault identification and classification of rotor winding asymmetries in WRIM. Moreover, a study of the influence of the sensor position on the results is included in the paper. This study enables to objectively measure the similarity between the obtained results at certain flux sensor positions, which are well-justified by the preponderance of certain flux components at those positions.

II. Theoretical Foundations: Bicoherence and Higher Order Spectra

The bispectrum is a higher resolution spectral technique that provides supplementary information about the amplitude and phase of the analyzed signal's components; it provides information regarding specific interactions between the different frequency components of that signal. More specifically, the bispectrum informs about the nonlinear interactions in the process that generates a signal. This can be especially useful when analyzing transient stray flux signals with fault diagnosis purposes. The mathematical definition of the bispectrum is as follows:

For a real discrete signal $\{x(n)\}, n = 0, \pm1, \pm2, \pm3$ ..., the third order cumulant is given by (1) [19].

$$C_{3x}(\tau_1, \tau_2) = \frac{1}{N}\sum_{n=N1}^{N2} x(n) \cdot x(n+\tau_1) \cdot x(n+\tau_2) \quad (1)$$

where N_1 y $N_2$are chosen in such a way that the summation involves only *x(n)* with $n \in [0, N-1]$, N is the number of samples in the cumulant region to be evaluated. Likewise, the bispectrum is defined by the Fourier Transform of the third order cumulant, which is given by [20]:

$$B(f_1, f_2) = \sum_{\tau_1=-N-1}^{N-1}\sum_{\tau_2=-N-1}^{N-1} C_{3x}(\tau_1, \tau_2) \cdot e^{-2\pi f_1 \tau_1} \cdot e^{-2\pi f_2 \tau_2} = \frac{1}{N^2} X(f_1, f_2) \cdot X(f_1) \cdot X(f_2) \quad (2)$$

where $X(f)$ is the Fourier Transform of the sequence $\{x(n)\}_{n=0}^{N-1}$.

The bispectrum in spectral domain can be computed through the convolution theorem ($X$is the Fourier Transform and X^*its conjugate):

$$B(f_1, f_2) = X^*(f_1 + f_2) \cdot X(f_1) \cdot X(f_2) \quad (3)$$

in this work the use of the bispectrum absolute value of the stray flux signal is proposed. The discrete theoretical description is as follows:

$$(B_x^N(f)) = |B_x^N(f_1, f_2)|_i, \nabla i = 1, \dots, N \quad (4)$$

where N is the number of rows of the square matrix (NxN) obtained from the bispectrum. The obtained result in (4) is a NxN matrix that contains the frequency values of the amplitude bispectrum matrix of the analyzed stray flux signal.

In practical terms, the bispectral representations included in this paper should be interpreted as follows: each point of the bispectrum represents the interactions between the frequency components given by its respective coordinates (f1, f2). In the plots included in this paper, the frequencies have been previously normalized versus the sampling rate (f_s=5kHz), this is, 5 kHz is normalized to 1Hz, so the fundamental frequency of the stray flux signal, 50Hz, represents the frequency 0.01 in the domain of the bispectrum. Taking this into account, the point (0.01, 0.01) represents the interaction between the fundamental component and itself, when the bispectral analysis is carried out. Therefore, the traces appearing around that point represent interactions between the fundamental component and nearby components (as those amplified by the fault), as well as the mutual interactions between these latter components. The appearance of the bispectrum will be informative not only on the frequency content of the analyzed signal but also of the interactions between the respective components, which yields much more information. In this paper, the bispectral representations are depicted through contour plots that depict the lines connecting similar values (in this case, the local maxima), using the same color.

A. *Bicoherence and Fuzzy C-Means Algorithm*

Bicoherence can be interpreted as an automatic index that can be calculated from a single signal. It takes values between 0 and 1, which makes it a convenient measure to quantify the degree of phase coupling in a signal. Then, the Bicoherence, according to equation (3), is defined as:

$$bic^2(f_1, f_2) = \frac{|B(f_1,f_2)|^2}{E[|X(f_1)\cdot X(f_2)|^2]E[|X^*(f_1+f_2)|^2]} \quad (5)$$

where the numerator contains the square magnitude of the bispectrum in all segments of the time series and the denominator is the factor that normalizes the bispectrum. Then, $0 \leq B(f_1, f_2) \leq 1$. The fuzzy C-Mean automatic classification algorithm is applied to the result of the above equation (5), which is defined as [21]:

$$J_m = \sum_{i=1}^{D} \sum_{j=1}^{N} u_{ij}^m \left\| x_i - c_j \right\|^2 \quad (6)$$

where D is the number of data points, N is the number of clusters, m is the fuzzy partition matrix exponent, x_i is the data points to evaluate, c_j is the cluster center of the j cluster and u_{ij} is the degree of membership of the data points x_i in the cluster.

The goal of the algorithm is to minimize the function (equation (6)). After the first iteration, the estimation of J_m gets smaller in value quantitatively, which means that the algorithm is approaching a decent split of the points associated with the ranking groups.

III. Experiments

In order to capture the stray flux data under starting, an experimental test bench was used (see Fig. 2). It was based on a 4P, 400V, 11kW WRIM that could operate under different load conditions. The WRIM was started by inserting a starting rheostat to decrease the starting currents (see blue element in Fig. 2). The rotor winding asymmetry was forced by inserting an additional external rheostat in series with one of the rotor phases (see yellow element in Fig.2). This additional rheostat enabled to insert up to ten levels of resistance (steps from 0.14 Ω to 11.6 Ω), so that different rotor fault severities were obtained (in this work, only two asymmetry levels are shown: moderate asymmetry (added resistance R_{add}=1.6 R_R with R_R=rotor winding resistance) and severe asymmetry (added resistance R_{add}=1.9 R_R) [3], [9]). Note that, since during the starting the starting rheostat was inserted, the effective value of the rotor phase resistance was higher than R_R. Also, note that a certain level of eccentricity was measured in the machine, even at healthy condition of the rotor winding (R_{add}=0). Several startups were carried out. The stray flux data under starting was obtained by registering the emf waveforms induced in an external coil sensor with 1,000 turns and with an external diameter of 80mm and an internal diameter of 39mm. The sampling rate was 5 kHz. The waveforms of the emf signals captured at each sensor position and after each tested rotor

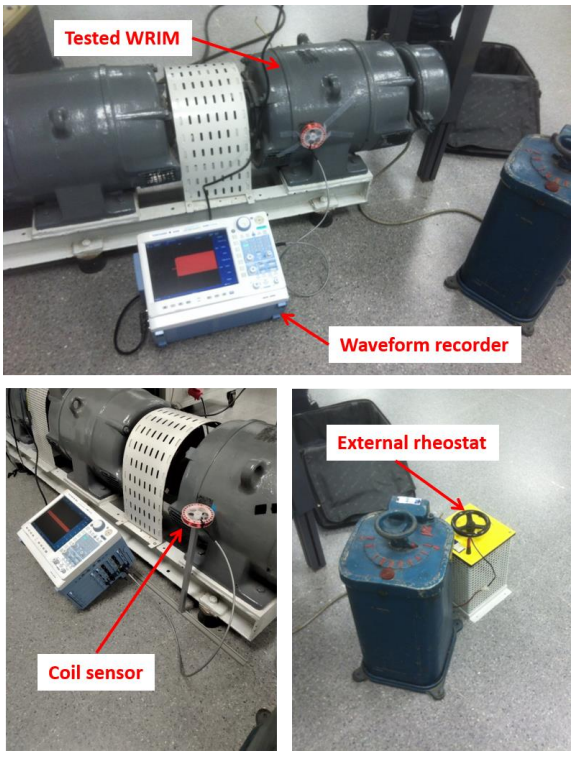

Fig. 2 Laboratory Test Bench.

winding condition are displayed in Fig,4. After capturing the emf waveforms, these were transferred to a computer, in which an algorithm enabling the application of the bispectrum was employed.

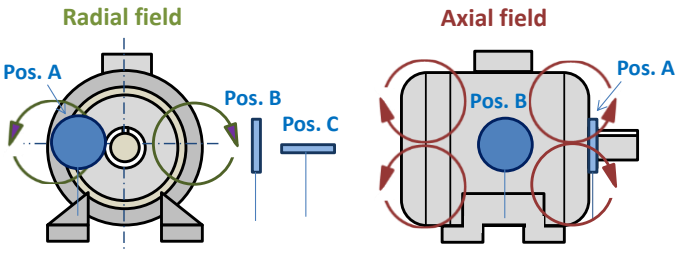

Fig. 3. Considered sensor positions for the experiments.

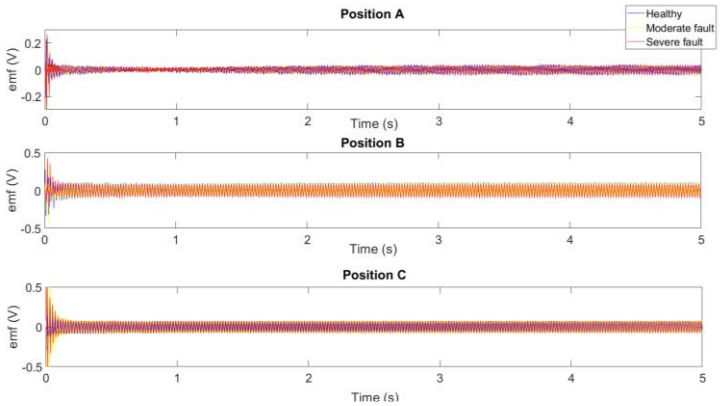

Fig. 4. Waveforms of emf signals for each sensor position and rotor winding condition.

IV. Results

Figs. 5 to 13 show the contour plots corresponding to the bispectra of the stray flux signals captured under starting for the three different sensor positions A, B and C, respectively (see Fig.3) and for several levels of rotor winding asymmetry ranging from healthy to level 2 (severe asymmetry). For the calculation of both the bispectrum and the bicoherence (which will be shown later), 512 samples have been used for each position and for each winding condition. This number of samples is sufficient to identify the different levels of failure, as well as to classify the results. As observed in Figs 5 to 7 (position A), the depth level in the contour plots increases as the level of asymmetry does, which reflects the appearance of new frequencies related to the fault (the fault components' frequencies change under starting, adopting values between 0 and the supply frequency). Note that, in healthy condition some traces are detected in the bispectra, which are caused by the certain eccentricity measured in the machine. However, the pattern is totally different from that at faulty condition. Figure 7 shows that, when the level of severity is the highest, there is a maximization of the contours, which is illustrated through the appearance of new circles. These represent, under a spectral point of view, new frequencies with significant amplitudes that are yielded by the fault that cause new interactions between these components and between them and the fundamental.

The same reasoning stands for position B, as shown in Figs. 8 to 10. Note that there are clear differences between the healthy and faulty bispectra at that sensor position. In healthy conditions, only the fundamental component and inherent eccentricity components. Note how the interactions are mainly located in the low frequency region, which is coherent with the expected location of the components amplified by eccentricities as suggested in recent works. But in the case of rotor winding asymmetry, additional interactions can be observed. Note the clear amplification of the contour plots around the fundamental (coordinate 0.01, 0.01 and symmetrical) that reveal higher interactions between the fundamental and nearby components. Note also the appearance of new contours, as the fault increases, which reveal the interactions between new components present in the signal.

All these interactions, reflected through the contour plots in the bispectra., yield characteristics signatures that can be automatically detected by intelligent algorithms to diagnose the fault.

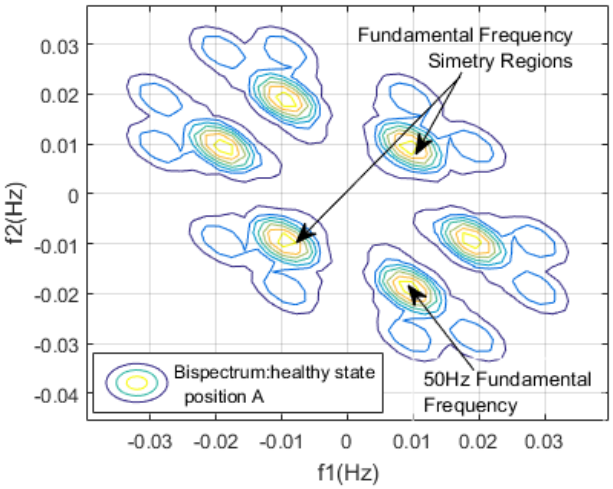

Fig. 5. Bispectrum of stray-flux signals under starting for the sensor position A (Healthy rotor).

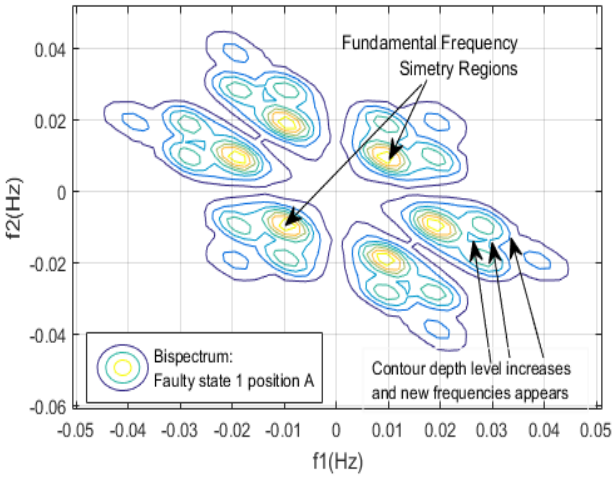

Fig. 6. Bispectrum of stray-flux signals under starting for the sensor position A (Rotor Asymmetry Level 1).

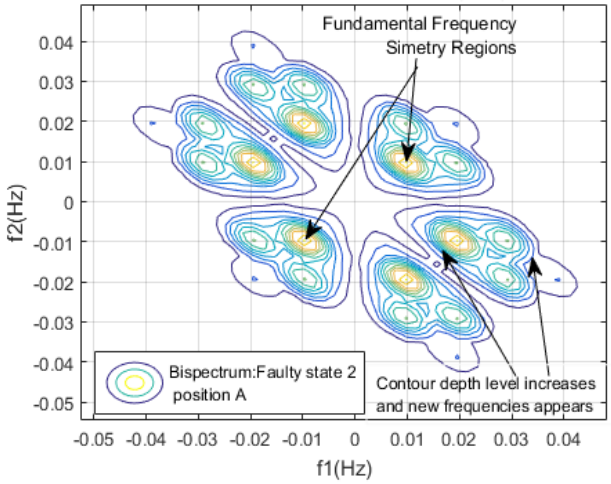

Fig. 7. Bispectrum of stray-flux signals under starting for the sensor position A (Rotor Asymmetry Level 2).

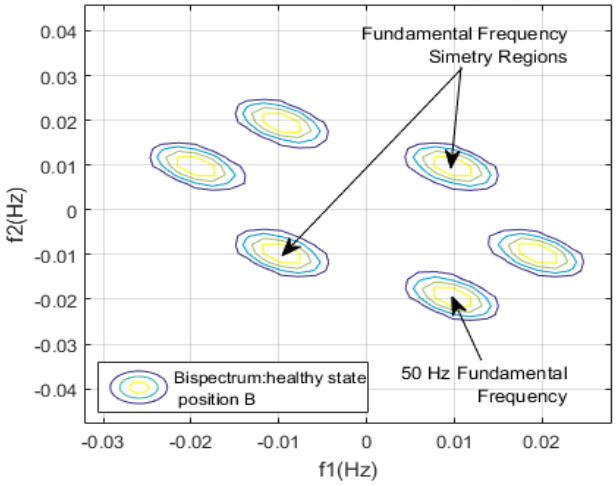

Fig. 8. Bispectrum of stray-flux signals under starting for the sensor position B (Healthy rotor).

The case of sensor at position C is especially evident, showing a progressive increment in these interactions between components as the rotor asymmetry increases, which can be directly observed in the plots. This is due to the fact that in this position, the *f·(1-2·s)* component is especially relevant, due to its radial nature, yielding more evident interactions compared to other positions. The results are shown in Figs. 11 to 13, respectively.

These figures reveal that there are qualitative differences between the bispectra for different sensor positions. However, there are individual identifiable common features that allow the discrimination between healthy and winding asymmetry cases for all sensor positions.

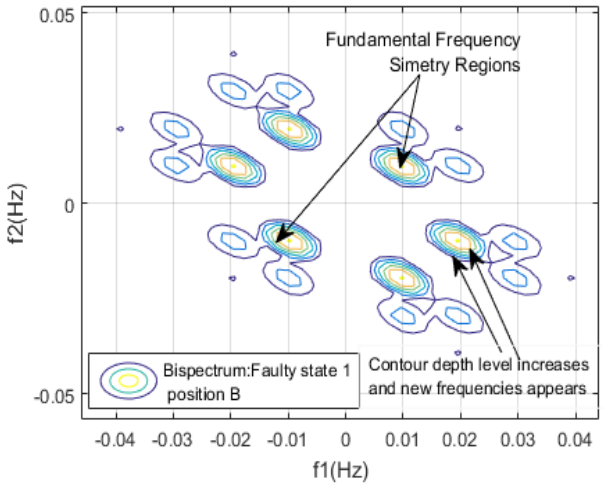

Fig. 9. Bispectrum of stray-flux signals under starting for the sensor position B (Rotor Asymmetry Level 1).

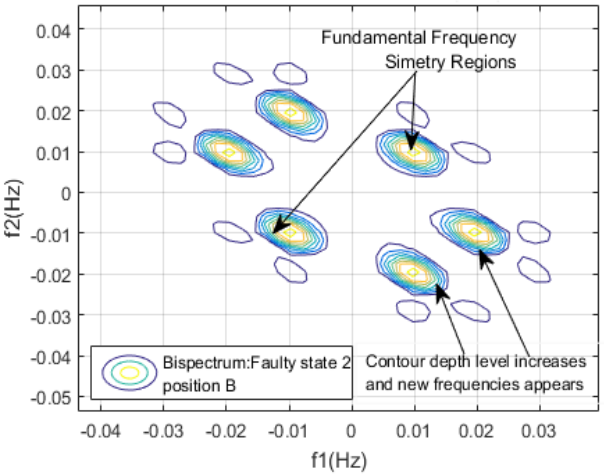

Fig. 10. Bispectrum of stray-flux signals under starting for the sensor position B (Rotor Asymmetry Level 2).

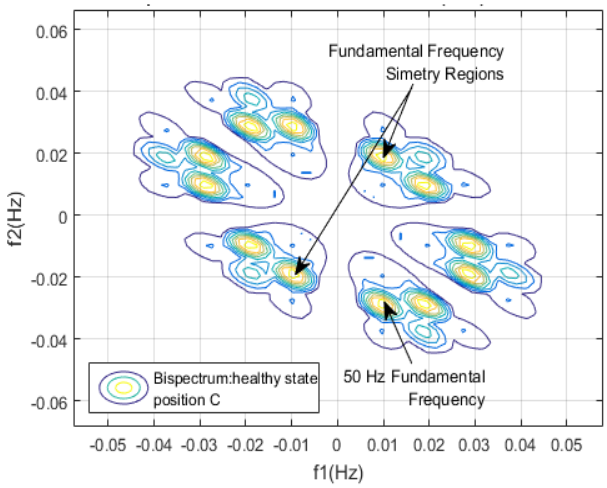

Fig. 11. Bispectrum of stray-flux signals under starting for the sensor position C (Healthy rotor).

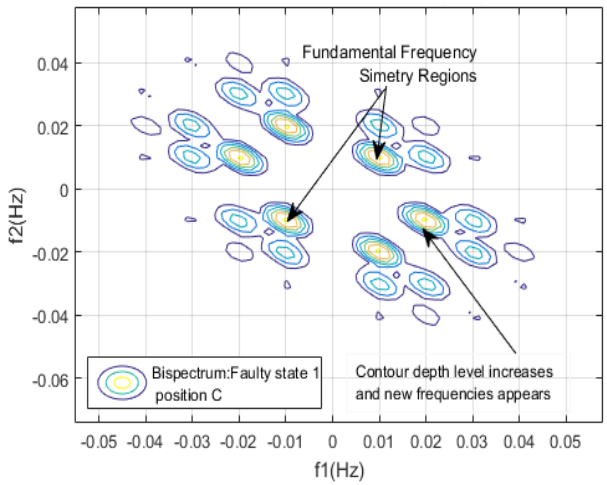

Fig. 12. Bispectrum of stray-flux signals under starting for the sensor position C (Rotor Asymmetry Level 1).

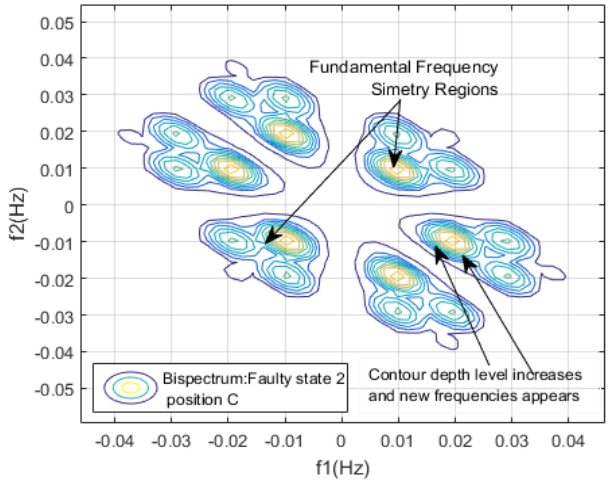

Fig. 13. Bispectrum of stray-flux signals under starting for the sensor position C (Rotor Asymmetry Level 2).

A. Clustering based on Fuzzy C-Mean of Bicoherence

The bispectrum provides information about the spectral content of the stray flux signals as well as of the different levels of failure according to the depth level of the contours. Based on this, in a real application, it is convenient to have algorithms that automatically determine the state of the motor according to its spectral content.

As the fault severity increases, new frequencies with random phases are generated in the transient stray flux signal; these may be coupled or not. To quantify this dispersion, the use of the Bicoherence is proposed; moreover, the Fuzzy C-Means unsupervised classification algorithm is employed to perform the automatic classification. Figs. 14 to 22 illustrate this process, by showing the cluster assignments and centroids for the different fault levels and for the three sensor positions. The peaks appearing in these graphs give an idea of the frequency concentration based on the identified groups raising from the respective bispectra. Therefore, they are a measure of the frequency dispersion for each case.

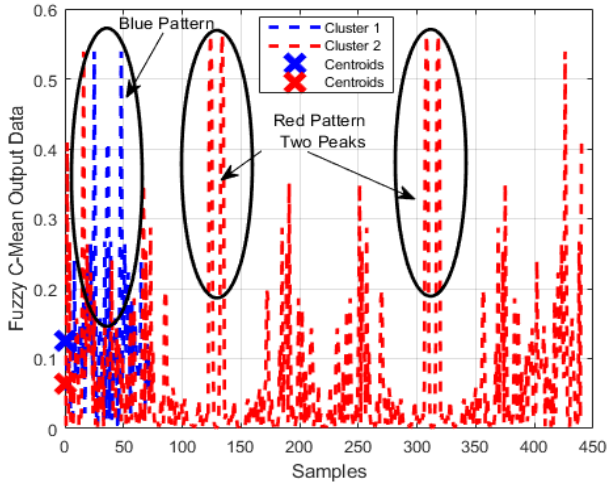

Fig. 14. Cluster Assignments and Centroids for Position A (Healthy rotor).

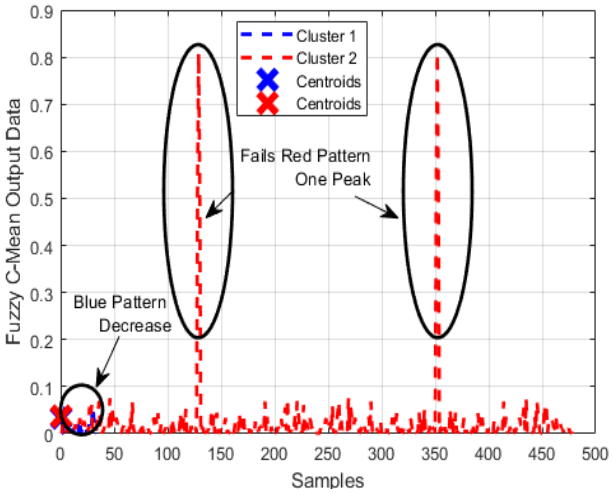

Fig. 15. Cluster Assignments and Centroids for Position A (Rotor Asymmetry Level 1).

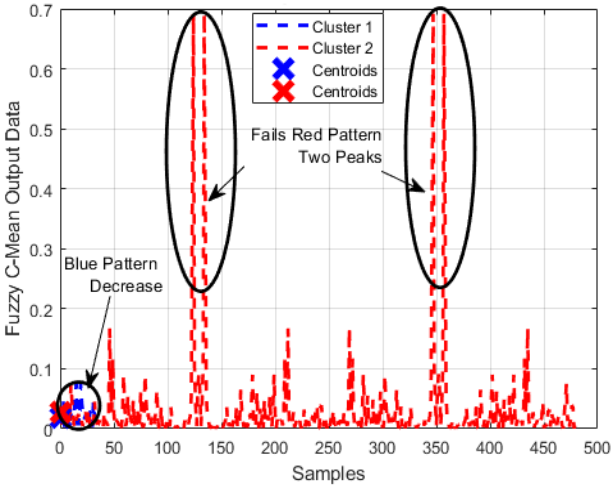

Fig. 16. Cluster Assignments and Centroids for Position A (Rotor Asymmetry Level 2).

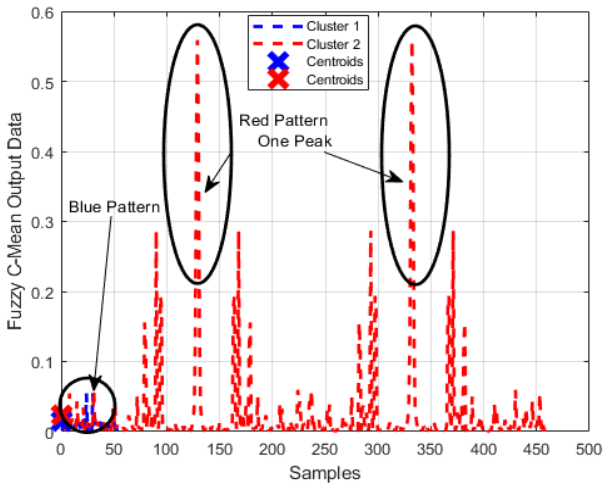

Fig. 17. Cluster Assignments and Centroids for Position B (Healthy rotor)

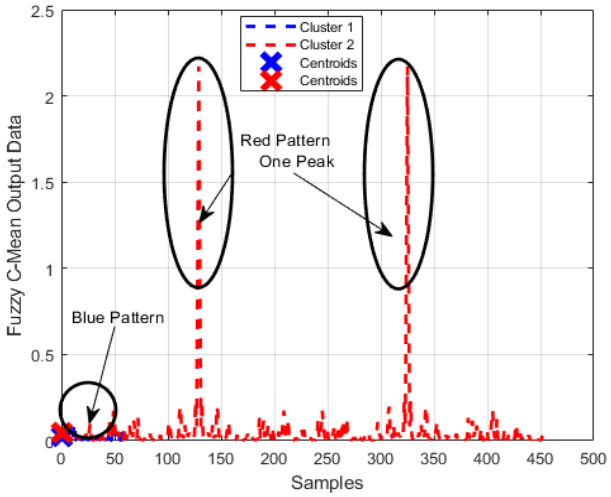

Fig. 20. Cluster Assignments and Centroids for Position C (Healthy rotor).

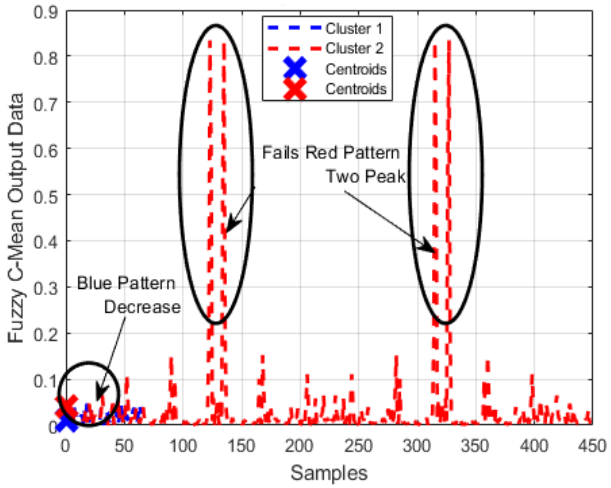

Fig. 18. Cluster Assignments and Centroids for Position B (Rotor Asymmetry Level 1).

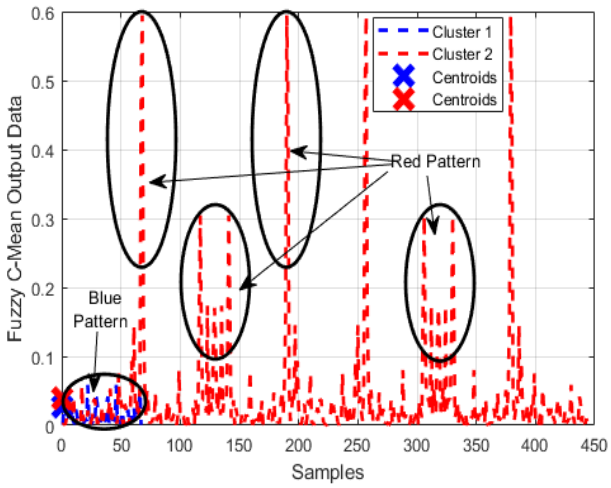

Fig. 21. Cluster Assignments and Centroids for Position C (Rotor Asymmetry Level 1).

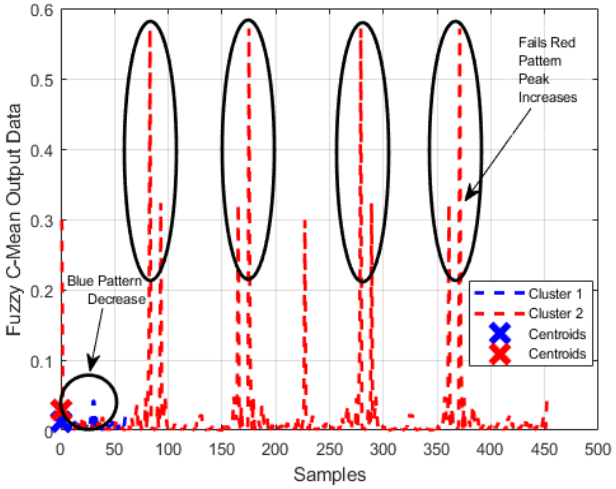

Fig. 19. Cluster Assignments and Centroids for Position B (Rotor Asymmetry Level 2).

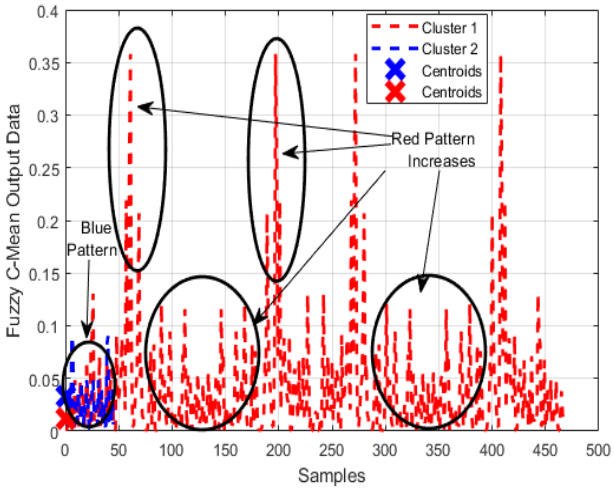

Fig. 22. Cluster Assignments and Centroids for Position C (Rotor Asymmetry Level 2).

Figs. 14 to 16 show that, for the sensor position A, the blue pattern decreases as the fault severity increases (see differences between rotor asymmetry cases and healthy condition). On the other hand, the red pattern shows an inconsistent trend for this position: it shows two peaks for the healthy case, one for the fault severity 1 and, again, two peaks for the fault severity 2. This erratic trend may be due to the fact that, at that sensor position, the main fault components are the axial ones (e.g. $s \cdot f$) and they are also present in healthy condition due to inherent eccentricity in the machine. This, together with the reduced amplitude of the captured stray flux signals at that position (which yields a low signal to noise ratio) causes this inconsistency in the results.

On the contrary, at position B and C the cluster assignment and classification results are more consistent. Figs. 17 to 19 (position B) show that a single peak pattern appears for the healthy case, whereas two-peak patterns raise for the different rotor winding asymmetry conditions. At position C (Figs. 20 to 22), a multiple peak red pattern appears for the faulty cases, showing clear differences with the single-peak pattern of the healthy case. Moreover, the blue pattern also increases its amplitude. The results for these positions are attributed to the higher differences yielded by the amplification of the radial components, such as $f \cdot (1\text{-}2 \cdot s)$) which evolves under starting across the whole frequency band below the fundamental.

All in all, these results prove a higher consistency of the results at sensor positions B and C that is justified on the irruption of multiple frequencies below the fundamental due to the evolution of the radial components, that are mostly captured at those positions.

In Section V, a study is carried out to determine how the sensor position influences the obtained results. The study is based on the analysis of the level of similarity and correlation between their respective results. To this end, the Pearson correlation coefficient, the squared magnitude coherence and the Wavelet coherence of each of the signals are used.

B. Comparison with other clustering methods

To illustrate the performance of the Fuzzy C-Means method, a comparative study with other clustering method is performed in this Section. The comparison is carried out in terms of execution time and error rate calculation. Other variants of fuzzy means algorithms are considered, namely:

- Classic Fuzzy C-Means (FCM)
- *General Type 2 FCM algorithm (GT2-FCM)* [22]
- Interval T2 F*uzzy C-means* (IT2-*FCM*) [23]
- Possibilistic *C-Means (PCM)* [24]

Since the algorithm and its variants are parametric need to know a priori the number of clusters implicit in the data. In this case the experiment was carry on with three cluster.

Fig. 23 and Table I show that the execution time for the classical variant of Fuzzy C-Means algorithm is the best. On the other hand, Table I reveals that the Possibilistic C-Means variants has the best success rate, although all approaches yield quite similar results. This justifies the use of Fuzzy C-Means since the classification performance is similar to that of other approaches while the execution time is much better.

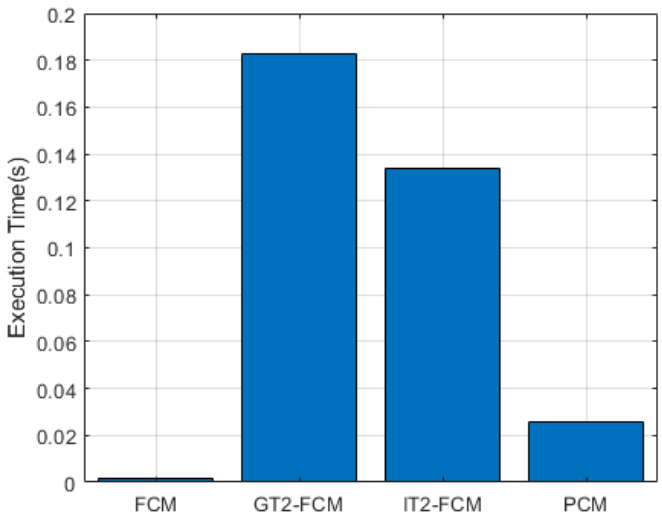

Fig. 23 CPU time comparison between every variants of Fuzzy Means Algorithm

Table I. Comparative analysis between different clustering methods

Algorithm	**Error Sample Count**	**Success Rate**	**Execution Time**
Fuzzy C-Means	17	88.66 %	0.001414
General Type 2(FCM)	16	89.33 %	0.110677
interval T2 (FCM)	17	88.66%	0.036101
Possibilistic C-Means	14	90.66%	0.021295

V. Mean Square Coherence: Influence of the Sensor Position

The discrepancies between the obtained results at each sensor position (especially between position A and positions B-C) are mainly attributed to the differences between the features of the respective stray-flux signals measured at each position. The main reason for existence of these differences relies, as explained in the paper, in the different nature of the components that are amplified by the fault at each considered position (axial at position A, radial at position C and, combined (axial + radial) at position B). This section is aimed to provide objective indicators of these differences between the stray-flux signals at different positions in three different dimensions, namely: time, frequency and time-frequency. To this end, the Pearson correlation coefficient, the squared magnitude coherence and the Wavelet coherence are respectively used.

The squared magnitude coherence can be estimated as a quantification measure of the relationship between two vectors; it is a function of the power spectral density $P_{xx}(f)$ and $P_{yy}(f)$, and the cross power spectral density $P_{xy}(f)$, of x and y, respectively [25].

$$C_{xy}(f) = \frac{P_{xy}(f)}{P_{xx}(f) \cdot P_{yy}(f)} \tag{7}$$

Since the coherence measures the relationship at the level of each frequency point in two vectors, the output $C_{xy}(f)$ is a vector that contains the existing correlation values at each frequency point for each pair x, y. In this case, each pair corresponds to each sensor position A, B and C, respectively, taken two by two. Table II shows the obtained results using the Pearson correlation coefficient and the Mean Coherence.

TABLE II. PEARSON CORRELATION AND MEAN COHERENCE BETWEEN EACH SENSOR POSITION (A,B AND C) IN THE HEALTHY STATE

PAIRS POSITIONS	PEARSON CORRELATION	MEAN COHERENCE
A-B	0.0575	0.2115
A-C	0.0210	0.2895
B-C	-0.7950	0.3675

The results of Table II show that there is a little relation, under a temporal point of view, between the stray flux signal measured at position A and those measured at positions B and C (note the reduced values of Pearson correlation coefficient), all of them corresponding to a healthy rotor condition. On the contrary, there is a high similarity between the signals captured at positions B and C (the Pearson coefficient yields a value of -0.7950).

Regarding the relationship of the spectral content, the hypothesis that positions B and C are related is strengthened, since a coherence value of 0.3675 is obtained, while the positions A-B and A-C are related in a lesser extent.

To show in detail the behavior of each frequency and phase and illustrate a classification by groups, which allows to identify a spectral pattern that justifies the automatic classification groups evaluated and obtained in each series, the wavelet squared magnitude coherence is used. Unlike the coherence based on the Fourier transform (see (7)), the Wavelet coherence is based on the Wavelet Transform and is used to evaluate a time-frequency analysis between the variables. Figs. 24 to 26 show the obtained results.

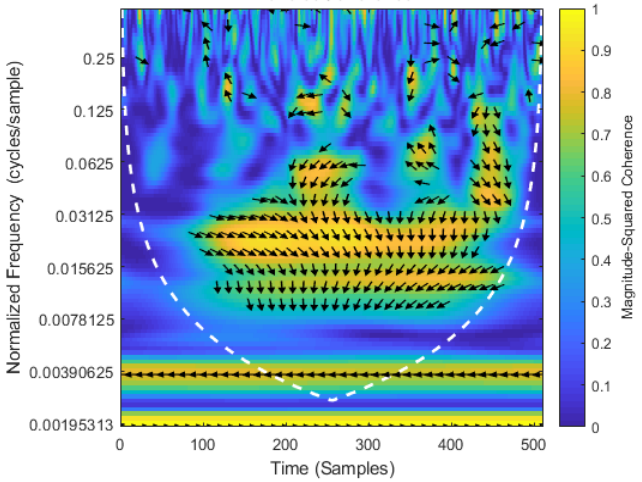

Fig. 24. Time-frequency Analysis based on Wavelet coherence, for Position A-B (Healthy rotor).

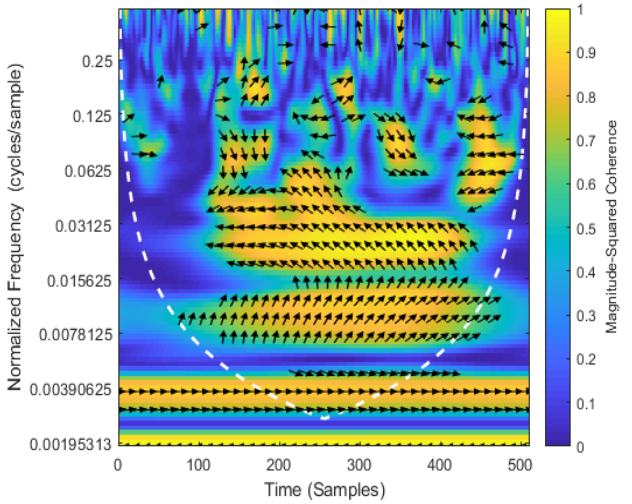

Fig. 25. Time-frequency Analysis based on Wavelet coherence, for Position A-C (Healthy rotor).

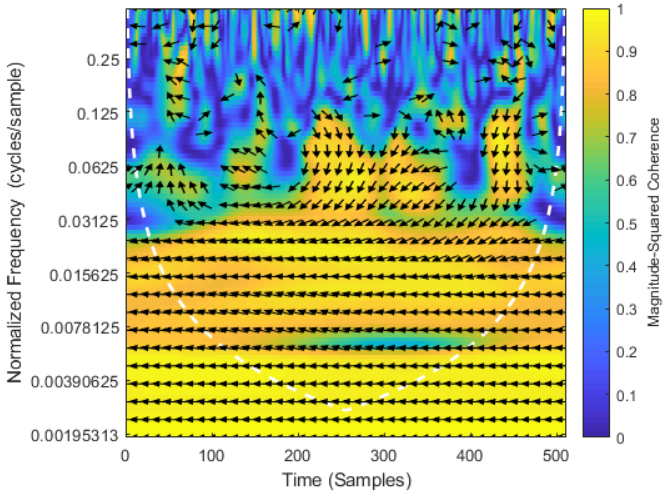

Fig. 26. Time-frequency Analysis based on Wavelet coherence, for Position B-C (Healthy rotor).

The cone of influence (dashed white line) indicates where edge effects occur in the consistency data. Due to edge effects, less credit is given to the areas of apparent high coherence that are outside the cone of influence or overlapping it.

The phase arrows (in black) represent the lead / lag phase relationships between the two data series, this is, it indicates if, in addition to coinciding in frequency, they also coincide in phase.

The pattern for positions A-B and A-C respectively is similar between the sample interval 100 to 400, but opposite in phase, which influences the classification.

The relationship that exists between position B and C respectively is significant in frequency and with the same phase. Hence, the classification patterns obtained for positions B and C respectively are similar and identify the faults in an appreciable way.

In conclusion, the following aspects are derived from the analysis carried out in this section:

- As shown in Table II, the correlation coefficient (that accounts for the similarity between temporal waveforms of the stray-flux) and the mean coherence (that accounts for the

similarity between spectral components) show a much higher similarity between B and C and a much more reduced similarity between these positions and position A (probably due to the higher presence of the radial components on the measured flux portion of the two first positions).

- The wavelet coherence, that is used to measure the similarities between the respective time-frequency maps, also reveals high similarities between positions B-C and much lower with respect position A, which is in agreement with the previous considerations.

All the previous facts serve to explain the different behaviors of the previous bispectra and, more specifically, the different patterns at position A versus those reached at positions B and C.

VI. Conclusion

In the present work, an algorithm for the automatic classification of rotor winding asymmetries in WRIM is proposed. It is based on the use of the Bicoherence of the stray flux signals under starting. Moreover, a method for unsupervised classification based on fuzzy logic is presented. For each analyzed sensor position, notable differences are found between healthy and faulty condition, reflected through common patterns appearing in the bispectra and that yield clear differences in the subsequent cluster assignments for healthy and faulty conditions. These facts prove the validity of the methods for identifying and classifying the asymmetries.

The performance of the proposed Fuzzy C-Means approach performance is compared to those of other methods. The comparison shows a much shorter computational time of the proposed approach that enables maintaining the classification accuracy of other methods.

In addition, an analysis about the influence of the sensor position in the fault detection process is carried out. It studies the correspondence and similarity of the measurements regardless of the position where the measurement is taken.

It is possible to identify that two of the three relative positions used in the experiments (B&C) present common characteristics; this was derived from the time-frequency analyses based on the coherence and the correlation coefficient. The obtained results confirm that the position of the sensor has a strong influence on clearly detecting the asymmetry, being B and C more suitable for automatic fault classification purposes.

Future works will deep in the discrimination between eccentricities and rotor asymmetries in WRIM, forcing more severe eccentricity levels and analyzing in detail the different repercussions that each fault has on the stray-flux spectrum plots.

References

[1] TECO-Westinghouse Motor Company. “Wound rotor motor technology”, http://www.tecowestinghouse.com/PDF/woundrotor.pdf

[2] P. Tavner, et al, “Condition Monitoring of Rotating Electrical Machines”, IET Power and Energy Series 56, United Kingdom, 2008

[3] J. Antonino-Daviu, *et al*, "Reliable Detection of Rotor Winding Asymmetries in Wound Rotor Induction Motors via Integral Current Analysis," in *IEEE Transactions on Industry Applications*, vol. 53, no. 3, pp. 2040-2048, May-June 2017.

[4] Y. Park, et al., "Airgap Flux based Detection and Classification of Induction Motor Rotor and Load Defects during the Starting Transient," in *IEEE Trans. on Ind. Electronics*, vol. 67, no. 12, pp. 10075-10084, Dec. 2020.

[5] A. Sapena-Bano, M. Riera-Guasp, R. Puche-Panadero, J. Martinez-Roman, J. Perez-Cruz and M. Pineda-Sanchez, "Harmonic Order Tracking Analysis: A Speed-Sensorless Method for Condition Monitoring of Wound Rotor Induction Generators," in *IEEE Transactions on Industry Applications*, vol. 52, no. 6, pp. 4719-4729, Nov.-Dec. 2016.

[6] Y. Gritli, C. Rossi, D. Casadei, F. Filippetti and G. Capolino, "A Diagnostic Space Vector-Based Index for Rotor Electrical Fault Detection in Wound-Rotor Induction Machines Under Speed Transient," in *IEEE Transactions on Industrial Electronics*, vol. 64, no. 5, pp. 3892-3902, May 2017.

[7] F. Vedreño-Santos, M. Riera-Guasp, H. Henao, M. Pineda-Sánchez and R. Puche-Panadero, "Diagnosis of Rotor and Stator Asymmetries in Wound-Rotor Induction Machines Under Nonstationary Operation Through the Instantaneous Frequency," in *IEEE Transactions on Industrial Electronics*, vol. 61, no. 9, pp. 4947-4959, Sept. 2014.

[8] J. A. Ramirez-Nunez *et al.*, "Evaluation of the Detectability of Electromechanical Faults in Induction Motors Via Transient Analysis of the Stray Flux," in *IEEE Transactions on Industry Applications*, vol. 54, no. 5, pp. 4324-4332, Sept.-Oct. 2018.

[9] I. Zamudio-Ramirez, *et al*, "Detection of winding asymmetries in wound-rotor induction motors via transient analysis of the external magnetic field," in *IEEE Trans. on Industrial Electronics*, vol. 67, no. 6, pp. 5050-5059, June 2020.

[10] B. Jang, C. Shin, E.J. Powers, W.M. Grady, Machine fault detection using bicoherence spectra, *in Proceedings of the 21st IEEE Instrumentation and Measurement Technology Conference*, 18-20 May 2004.

[11] Y. Li and S. Zhou, "A New Instantaneous Wavelet Bicoherence for Local Fault Detection of Rotating Machinery," in *IEEE Transactions on Instrumentation and Measurement*, vol. 69, no. 1, pp. 135-143, Jan. 2020.

[12] R. U. Maheswari and R. Umamaheswari, "Trends in non-stationary signal processing techniques applied to vibration analysis of wind turbine drive train—A contemporary survey", *Mech. Syst. Signal Process.*, vol. 85, pp. 296-311, Feb. 2017.

[13] M. A. Hassan, A. M. E. Bayoumi and Y. J. Shin, "Quadratic-nonlinearity index based on bicoherence and its application in condition monitoring of drive-train components", *IEEE Trans. Instrum. Meas.*, vol. 63, no. 3, pp. 719-728, Mar. 2014.

[14] Y. Larsen and A. Hanssen, "Wavelet-polyspectra: Analysis of non-stationary and non-Gaussian/non-linear signals in statistical signal and array processing", *Proc. 10th IEEE Workshop Stat. Signal Array Process.*, pp. 539-543, Aug. 2000.

[15] A. J. Gómez González, X. Rodríguez, A. Sagartzazu, A. Schumacher, and I. Isasa. “Multiple Coherence Method in Time Domain for the Analysis of the Transmission Paths of Noise and Vibrations with Non-Stationary Signals.” *Proceedings of the 2010 International Conference of Noise and Vibration Engineering*, ISMA2010-USD2010. pp. 3927–3941.

[16] D. Maraun,, J. Kurths, and M. Holschneider. "Nonstationary Gaussian processes in wavelet domain: Synthesis, estimation and significance testing.” Physical Review E 75. 2007, pp. 016707-1–016707-14.

[17] T. Ciszewski, L. Gelman, A. Ball, “Novel Fault Identification for Electromechanical Systems via Spectral Technique and Electrical Data Processing” *Electronics* 2020, 9, 1560.

[18] M. E. Iglesias-Martínez, P. Fernández de Córdoba, J. A. Antonino-Daviu and J. Alberto Conejero, "Bispectrum Analysis of Stray Flux Signals for the Robust Detection of Winding Asymmetries in Wound Rotor Induction Motors," *2020 IEEE Energy Conversion Congress and Exposition (ECCE)*, Detroit, MI, USA, 2020, pp. 4485-4490

[19] Mendel, J.M. Tutorial on higher-order statistics (spectra) in signal processing and system theory: Theoretical results and some applications. *Proc. IEEE*, 1991, 79, 278–305.

[20] Nikias, C.L., Mendel, J.M.: Signal Processing with Higher-Order Spectra. *IEEE Signal Processing Magazine* 10(3), 10–37 ,1993

[21] J.C. Bezdek, R. Ehrlich, W. Full, “FCM: The Fuzzy c-Means Clustering Algorithm”. *Computers & Geosciences* 10 (2-3): 191-203. 1984.

[22] O. Linda and M. Manic, "General Type-2 Fuzzy C-Means Algorithm for Uncertain Fuzzy Clustering," in IEEE Transactions on Fuzzy Systems, vol. 20, no. 5, pp. 883-897, Oct. 2012.
[23] C. Hwang and F. C. Rhee, "Uncertain Fuzzy Clustering: Interval Type-2 Fuzzy Approach to C-Means," in IEEE Transactions on Fuzzy Systems, vol. 15, no. 1, pp. 107-120, Feb. 2007.
[24] R. Krishnapuram and J. M. Keller, "The possibilistic C-means algorithm: insights and recommendations," in IEEE Transactions on Fuzzy Systems, vol. 4, no. 3, pp. 385-393, Aug. 1996.
[25] S. Malekpour, J.A. Gubner, W.A. Sethares, "Measures of generalized magnitude-squared coherence: Differences and similarities", Journal of the Franklin Institute, Vol. 355, no.5, 2018, pp.2932-2950.

Miguel Enrique Iglesias Martínez was born in Pinar del Río Cuba in 1984. He obtained a degree in Telecommunications and Electronics Engineering from University of Pinar del Río (UPR) in 2008, and a Master's Degree in Digital Systems at the Technological University of Havana, Cuba, in 2011. In 2020 he received his PhD in Mathematics at Universitat Politècnica de València. Currently works at the, University of Pinar del Rio and he is associate researcher at InterTech Interdisciplinary Modeling Group from Instituto Universitario de Matemática Pura y Aplicada at Universitat Politècnica de València. He is member of the group Psychological development, health and society - PSDEHESO from Universitat de València. His areas of research interest are Signal Processing, Noise Analysis and Blind Information Extraction, as well as Pattern Recognition Systems. Dr. Iglesias-Martínez was recipient of four scientific prizes from the Cuba Academy of Sciences in the years 2011, 2012, 2015, and 2017.

Jose A. Antonino-Daviu (S'04–M'08–SM'12) received the M.S. and Ph.D. degrees in electrical engineering from the Universitat Politècnica de València, Valencia, Spain, in 2000 and 2006, respectively, and the B.S. degree in business administration from the Universitat de Valencia, Valencia, in 2012. He was with IBM for two years, being involved in several international projects. He is currently an Associate Professor with the Department of Electrical Engineering of the mentioned university, where he develops his docent and research work. He was an Invited Professor with the Helsinki University of Technology, Finland, in 2005 and 2007, Michigan State University, USA, in 2010, Korea University, South Korea, in 2014, and the Université Claude Bernard Lyon 1, France, in 2015. He has authored or coauthored more than 200 contributions, including international journals, conferences, and books. Dr. Antonino-Daviu is an Associate Editor for IEEE TRANSACTIONS ON INDUSTRIAL INFORMATICS, IEEE INDUSTRIAL ELECTRONICS MAGAZINE and IEEE Journal of Emerging and Selected Topics in Industrial Electronics. He is also IEEE Industry Applications Society Distinguished Lecturer for 2019–2021. He was the General Co-Chair of IEEE International Symposium on Diagnostics for Electric Machines, Power Electronics and Drives 2013. He was recipient of the Nagamori Award from Nagamori Foundation, Kyoto, Japan, in 2018, for his contributions in electric motors transient analysis area. He was also recognized with the SDEMPED Diagnostic Achievement Award in Toulouse, France, 2019 and with the Medal of the Spanish Royal Academy of Engineering in 2016.

Pedro Fernández de Córdoba was born in Valencia in October 1965. He received the B.Sc., M.Sc., and Ph.D. degrees in physics from the Universitat de València (UV), Valencia, Spain, in 1988, 1990, and 1992, respectively. He also received the Ph.D. degree in mathematics from the Universidad Politécnica de Valencia (UPV), Valencia, in 1997. His research work was performed at UV, UPV, the Joint Institute for Nuclear Research (Russia), the University of Tübingen (Germany), and the Istituto Nazionale di Fisica Nucleare, Torino, Italy, among others. He is currently a Professor with the Department of Applied Mathematics, UPV. His research interests include the area of modeling and numerical simulation of physical and engineering problems, mainly focusing on the nu- merical treatment of heat and mass transfer problems. Dr. de Córdoba is Doctor Honoris Causa from the University of Pinar del Rio (Cuba), a member of the Colombian Academy of Exact, Physical and Natural Sciences, a member of the Académie Nationale des Sciences, Arts et Lettres du Bénin, Profesor Invitado of the University of Pinar del Rio, and Profesor Visitante "Ad Honorem" of the Universidad del Magdalena (Colombia). Furthermore, since its establishment on September 30, 2011, he has been a member of the Board of the Spanish Mathematics-Industry network (www.math-in.net).

J. Alberto Conejero received the B.Sc. and M.Sc. degree in mathematics from the Universitat de València (1998) and the M.Sc. degree in Bioinformatics and Biostatistics from Universitat Oberta de Catalunya and Universitat de Barcelona (2020). He obtained a Ph.D. degree in applied mathematics from the Universitat Politècnica de València, UPV, (2004) receiving the Outstanding Dissertation Award.
He is full professor at UPV since 2020. He is currently the Director of the Department of Applied Mathematics, UPV, and responsible for the M.Sc. program on Mathematics Research at UPV. He has been visiting scholar at Bowling Green St. University, USA; Kent St. University, USA; Università del Salento, Italy; Universität Tübingen, Germany; and Czech Academy of Sciences, Czech Republic. His research interests include dynamical systems, partial differential equations, graph theory, network science, and the multidisciplinary applications of mathematics to computer science, engineering, and biotechnology. Dr. Conejero was a recipient of the Teaching Excellence Prize of UPV in 2014, and he won the XPRIZE $500k Pandemic Response Challenge with VALENCIA IA4COVID team in 2021.

Larisa Dunai (M´19)**,** Associate Professor at UPV, obtained her MSc degree in Electronic Engineering in 2003 from Technical University of Moldova and a Master degree in Electronic Engineering in 2004 at the same university. After obtaining the MSc degree joined the Technical University of Moldova as Assistant professor at the Radio electronics and Telecommunications Department. In 2007 she started working as a researcher in the Research Center in Graphic Technology (CITG) of the Universidad Politecnica de Valencia. In November 2008 she joined the UPV as an Assistant professor of Graphic Design Department. In 2010 obtained her PhD at Universitat Politècnica de València. In 2013 she received the MIT Innovators Award for Spain and in 2014 the Michael Richey Medal from Royal Institute of Navigation.